LANGMUIR

pubs.acs.org/Langmuir Article

Probing the Structural Dynamics of the Coil–Globule Transition of Thermosensitive Nanocomposite Hydrogels

Renata L. Sala,* Tiago Venâncio, and Emerson R. Camargo*

Cite This: *Langmuir* 2021, 37, 1531–1541 Read Online

ACCESS | Metrics & More | Article Recommendations | Supporting Information

ABSTRACT: Nanocomposite hydrogels have emerged to exhibit multipurpose properties, boosting especially the biomaterial field. However, the development and characterization of these materials can be a challenge, especially stimuli-sensitive materials with dynamic properties in response to external stimuli. By employing UV–vis spectroscopy and NMR relaxation techniques, we could outline the formation and behavior of thermosensitive nanocomposites obtained by *in situ* polymerization of poly(*N*-vinylcaprolactam) (PNVCL) and mesoporous silica nanofibers under temperature stimuli. For instance, inorganic nanoparticles covalently linked to PNVCL changed the pattern of temperature-induced phase transition despite showing similar critical temperatures to neat PNVCL. Thermodynamic parameters indicated the formation of an interconnected system of silica and polymer chains with reduced enthalpic contribution and mobility. The investigation of water molecule and polymer segment motions also revealed that the absorption and release of water happened in a wider temperature range for the nanocomposites, and the polymer segments respond in different ways during the phase transition in the presence of silica. This set of techniques was essential to reveal the polymer motions and structural features in nanocomposite hydrogels under temperature stimuli, demonstrating its potential use as experimental guideline to study multicomponent nanocomposites with diverse functionalities and dynamic properties.

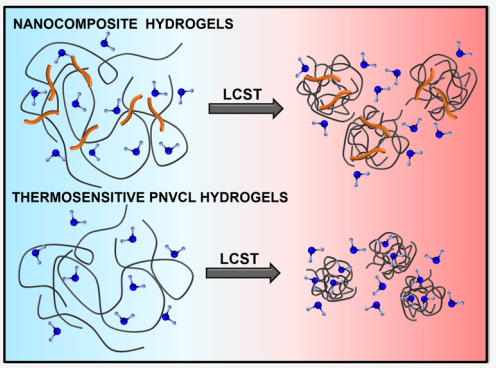

INTRODUCTION

Stimuli-sensitive hydrogels are designed polymers that respond to environmental changes such as temperature, pH, electric or magnetic field, light, and the presence of specific molecules and others.[1−3] Since they undergo conformational or chemical changes triggered by external stimuli, these materials can suit a myriad of applications in fields including controlled release and delivery of drugs, tissue engineering, diagnostics, sensors, intelligent coatings, and smart optical systems.[1,4] In special, hydrogels that respond to the physiological environment are crucial in the development of new biotechnologies. A highlight of this group is the biocompatible thermosensitive poly(*N*-vinylcaprolactam) (PNVCL) that forms physically cross-linked hydrogels above its lower critical solution temperature (LCST) around 34 °C, finding many applications as drug delivery systems,[5,6] entrapment of cells and enzymes,[7,8] tissue engineering,[9,10] as well as in smart devices.[11]

Despite the great potential of stimuli-sensitive hydrogels, some systems demonstrated low mechanical properties and relatively rapid release of hydrophilic drugs or inefficient incorporation of hydrophobic drugs, which may limit their application.[12−14] As an alternative, nanocomposites composed of multicomponent systems with diverse functionality within hybrid hydrogels have emerged, extending the prospects of biomaterial creation with specific molecular and physiological responses.[12] For instance, when inorganic nanoparticles are inserted into hydrogels, the nanocomposites can exhibit multiple functionalities by the association of the polymer network structure with the mechanical resistance, magnetic, electrical, and optical properties of inorganic nanoparticles.[15] In drug delivery systems, the incorporated nanoparticles can regulate the stimulus for drug release and enhance the loading, transport, and delivery of different types of drugs, contributing to the design of multifunctional nanocomposites.[12,16−18] For example, Koshy *et al.*[19] studied the adsorption of proteins in Laponite clay inserted into a hydrogel matrix, resulting in injectable nanocomposite carriers of proteins with sustained and localized delivery. In the case of PNVCL-based materials, Chang *et al.*[5] obtained bioresponsive silica nanoparticles loaded with anticancer drugs and coated with a sheddable polymer shell of cross-linked PNVCL copolymer engineered to respond to small variations in the physiological environment.

Although the synergistic combination of nanoparticles and hydrogels can perform unique properties, a deeper inves-

Received: October 22, 2020
Revised: January 7, 2021
Published: January 22, 2021

https://dx.doi.org/10.1021/acs.langmuir.0c03079
Langmuir 2021, 37, 1531–1541

tigation of the nanoparticle effect into the stimuli-responsive behavior of hydrogels is missing. For instance, depending on the amount of grafted polymers on the nanoparticle surface, the LCST can be tuned to different temperatures or even disappear when the systems lose the thermosensitive properties.[5,17,20−24] While most of these studies examined core/shell systems with thermosensitive polymers and inorganic nanoparticles, the resultant phase transitions are commonly overlooked and the interactions between the components are not clearly understood.[5,20−24]

Depending on the interactions of the components, nanocomposites can have their properties enhanced or even suppressed. For example, any variations in the hydrophilic and hydrophobic forces that govern the phase transition of thermosensitive hydrogels by the addition of an inorganic component could change the temperature-responsive behavior of the nanocomposites. When the polymer chains strongly interact with nanoparticles, there is a formation of an interfacial layer constituted by dangling polymer tails, adsorbed segments, and loops with significantly altered dynamics,[25] which properties are distinct from the bulk.[26−28] Accordingly, depending on the interfacial interactions, nanocomposites can have complex spatial configurations arising from polymer anchoring and adsorption on solid surfaces.[28,29]

Traditional nanoparticle-filled polymers are usually obtained as films, powders, or melted states and can be characterized by standard and well-known techniques. On the other hand, thermosensitive-based materials obtained in the form of hydrogels, core/shell nanoparticles, or multisensitive systems are regularly employed as aqueous suspensions and require adjustable techniques to analyze these complexes and dynamic systems in distinct environmental conditions. Some of these materials exhibit low mechanical properties and are composed of a multicomponent system, which can hamper the evaluation of their physicochemical properties and structural and morphological changes in response to stimuli. NMR spectroscopy has demonstrated to be a useful technique to provide information about the molecular motion of thermosensitive polymers in different solvents, medium conditions, and temperature ranges.[30] Through the employment of proton relaxation methods and the obtainment of spin−lattice relaxation time (T_1) and spin−spin relaxation time (T_2), it is possible to monitor the changes of polymer dynamics and the mobility of water molecules during the sol−gel transition, as well as in distinct heterogeneous structures.[31,32] While T_1 is especially related to local segmental motions, T_2 is described by large-scale motions.[33] For example, by investigating the T_2 value of PNVCL microgels with different amounts of cross-linker, Balaceanu *et al.*[34] identified a bimodal distribution of molecular dynamics inside the microgels, indicating that the materials had a heterogeneous core−corona internal structure. In a similar way, Etchenausia *et al.*[2] found two T_2 values for the methylene protons of PNVCL related to the core and shell structure of cationic PNVCL microgels. Similar studies and investigation of spin−spin relaxation time were also conducted with other PNVCL-based copolymers[35−38] and thermosensitive polymers.[39−43]

The hydrogel macromolecular motions are usually monitored by measuring T_1 and T_2 from a specific proton of the polymer chain or solvents. For instance, Spěváček *et al.*[44−46] monitored the T_2 value of water molecules during the phase transition of thermosensitive polymers at different temperatures and times. They found the existence of a portion of water molecules with a lower T_2 value above the T_{cp} value, corresponding to water molecules with spatially restricted mobility bound in the globular polymer state. Despite the great gain in molecular dynamics investigation with NMR relaxation experiments, few studies looked into T_1 values in details, which transcribe the local motion changes as a result of the rotation of main-chain bonds and intermolecular interactions, contributing to describe the overall macromolecular motion.[33,47] Additionally, the study and development of nanocomposites based on hydrogels and thermosensitive polymers could advance significantly since the local segmental and overall motions are greatly influenced by the presence of nanoparticles, modifying the resultant material properties. However, these systems still remain scarcely explored by NMR relaxometry,[48,49] opening new avenues to investigate the dynamic properties of stimuli-sensitive nanocomposites. In particular, it would boost the field of drug delivery systems designed to perform intermittent on-demand drug release, which have required the combination of two or more polymer and inorganic components as well as biomolecules.[50−52] To ensure optimal formulation and target application, the interactions between components have to be understood and how their properties will dynamically change over time in a physiological environment with physical and chemical cues.[53]

In this study, we were interested in understanding how multicomponent systems based on thermosensitive polymers dynamically behave under temperature stimuli by the evaluation of their thermodynamics and structural changes. We employed nanocomposites of thermosensitive PNVCL and functionalized mesoporous silica nanofibers as a model nanoparticle due to its wide range of biotechnological applications according to its biocompatibility and mechanical resistance. The high surface area and pore volume of mesoporous silica nanofibers can immobilize drugs, cells, contrast agents, fluorescent molecules, and other nanoparticles such as gold, finding applications in biocatalysis, biosensors, bioimaging, and drug delivery vehicles.[54−58] Additionally, the nanofiber shape has contributed to improve the mechanical and diffusion properties of hydrogels for tissue engineering applications.[59,60] We investigated these nanocomposites by UV−vis spectroscopy and NMR relaxation analysis in order to unveil the effect of nanoparticles in the temperature-induced phase transition of thermosensitive hydrogels. The outcomes of this work open new approaches to develop and characterize stimuli-responsive multifunctional systems with dynamic properties.

EXPERIMENTAL SECTION

Materials. All materials were used as received except the 2,2′-azobis(2-methylpropionitrile) initiator donated by DuPont (AIBN, DuPont, Brazil) that was previously recrystallized in methanol. *N*-Vinylcaprolactam monomer (NVCL, ≥98%), cetyltrimethylammonium bromide (CTAB, ≥99.5%), perfluorooctanoic acid (PFOA, 96%), and tetraethyl orthosilicate (TEOS, 98%) were purchased from Sigma-Aldrich Chemical Co. (USA). Sodium hydroxide (NaCl), toluene, hydrochloric acid (HCl), methanol (MeOH), and dimethyl sulfoxide (DMSO, p.a., ACS reagent) were purchased from Synth (Brazil). 3-(Trimethoxysilyl)propyl methacrylate (MPS, 98%) was purchased from Alfa Aesar (USA).

Synthesis of Mesoporous Silica Nanofibers (SiO_2). Mesoporous silica nanofibers were synthesized based on the methodology proposed by Rambaud *et al.*[54] Initially, 0.60 g of CTAB, 0.06 g of PFOA, and 2.30 mL of NaOH solution (2 M) were added and stirred in 300 mL of distilled water. Then, the temperature of the mixture

https://dx.doi.org/10.1021/acs.langmuir.0c03079
Langmuir 2021, 37, 1531−1541

was increased to 60 °C and 3.82 g of TEOS was added to the system and stirred for 2 h. The obtained mesoporous silica nanofibers were purified after being centrifuged at 7000 rpm for 4 min, washed in distilled water three times, and dried at 60 °C.

Later, the CTAB template was removed by acid−alcohol extraction.[61] One gram of SiO_2 was dispersed in 100 mL of methanol and 1.0 mL of HCl. The system was stirred and kept under reflux at 80 °C for 24 h, and the nanofibers were purified after being centrifuged at 7000 rpm for 4 min and washed in ethanol and distilled water until reaching neutral pH. After CTAB removal, silica nanofibers were functionalized with MPS. One gram of silica and 10 mL of MPS were dispersed in 100 mL of toluene and refluxed at 85 °C for 6 h.[62] The obtained silica mesoporous nanofibers were purified after being centrifuged at 7000 rpm for 4 min, washed in ethanol three times, and dried at 60 °C.

Synthesis of Nanocomposites. The nanocomposites were synthesized as similar described for PNVCL homopolymer.[62] One and five percentages (mass of silica/mass of monomer) of functionalized silica nanofibers and NVCL monomer were dispersed in dimethyl sulfoxide (15 wt %). The system temperature was increased to 70 °C, 2% AIBN (mass of initiator/mass of monomer) was added to the system, and the reaction proceeded for 4 h under a nitrogen atmosphere. The nanocomposites were purified after being centrifuged at 10,000 rpm for 1 min and resuspended in hot distilled water four times. Then, the nanocomposites were dried at 50 °C in a laboratory oven with forced air circulation.

Characterization. *Scanning and High-Resolution Transmission Electron Microscopies (SEM and HRTEM).* The morphology and size of mesoporous silica nanofibers were analyzed by SEM and HRTEM, as shown in Figure 1. The silica colloidal dispersions were dripped on

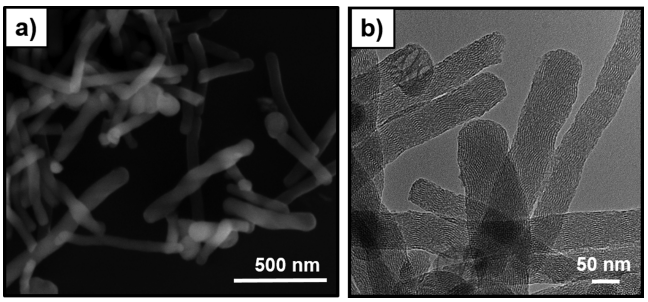

Figure 1. SEM (a) and HRTEM (b) images of functionalized mesoporous silica nanofibers.

copper grids covered with a thin amorphous carbon film to collect images in a TECNAI F20 field emission HRTEM operated at 200 kV and on silicon substrates to collect images in a JEOL JSM-5600LV operated at 20 kV.

UV−vis Spectroscopy. The transmittance of PNVCL and nanocomposite aqueous solutions (1% m/v) measured at the wavelength range (200−800 nm) from 25 to 36 °C was analyzed in a MultiSpec-1501 UV−vis spectrophotometer Shimadzu with a TCC-240A thermoelectrically temperature-controlled cell holder. The transmittance values of polymer and nanocomposite suspensions were analyzed every 0.5 °C, and the temperature was allowed to stabilize for 3 min before the measurement of the transmittance. To avoid any precipitation of the samples during the measurements, the material suspensions inside the cuvettes were constantly homogenized with a Pasteur pipette. The Mathematica 10 (Wolfram Research, Inc.) software package was used to calculate the thermodynamic parameters of polymer and nanocomposite systems by fitting the data of optical density variation as a function of temperature.

NMR Spectroscopy. Liquid-state NMR experiments were performed on a Bruker Avance III equipped with an Oxford 9.4 Tesla, with the related frequency of 400 MHz for the hydrogen-1 nucleus. Analyses were performed with a tunable probe for a wide range of frequencies (40−160 MHz) and with 5 mm diameter tubes. Spin−lattice (T_1) and spin−spin (T_2) relaxation times of PNVCL and its nanocomposites dispersed in 700 μL of deuterium oxide (5% m/v) were measured from 25 to 40 °C. T_1 values were determined by the inversion recovery method (rd−2θ−τ−θ−acq), where rd is the relaxation delay (70 s), 2θ and θ correspond to 180 and 90° pulses, respectively, and τ was linearly varied between 0.01 and 30 s. The acquisition time, acq, was 2.04 s, and 21 data points were collected to obtain the curve for fitting. T_2 measurements were done by the Carr−Purcell−Meiboom−Gill pulse sequence (rd−θ−[τ−2θ−τ]$_n$−acq), where rd was 43 s, τ was 1.0 ms, and the loop number, n, was linearly varied from 2 to 1500. The acquisition time, acq, was 2.04 s, and 16 data points were collected to reach the curve for fitting. For some conditions, biexponential functions of the normalized area integral of proton resonances ($I(\tau)$) versus echo time (τ) gave the best fit, revealing short (T_S) and long (T_L) relaxation times and the constants A and B (eq 1).

$$I(\tau) = A \exp\left(-\frac{\tau}{T_S}\right) + B \exp\left(-\frac{\tau}{T_L}\right) \quad (1)$$

Viscosity. The inherent viscosity of PNVCL and its nanocomposite aqueous solutions (1% m/v) was measured in an automated microviscometer Anton Paar (AMVn) in the temperature range of 25 to 40 °C. According to the increase in viscosity with temperature above the temperature-induced phase transition, the viscosity at 40 °C could not be measured. The intrinsic viscosities [η] were calculated by the Solomon−Ciuta equation (eq 2), where c is the concentration of the solution, t is the flow time of the polymer solution, and t_0 is the flow time of the solvent.[63,64] Then, the viscosity average molecular weights (M_v) were calculated by the Mark−Houwink−Sakurada equation (eq 3), using already reported parameters.[65]

$$[\eta] = \frac{\sqrt{2 \times \left(\frac{t}{t_0} - \ln\frac{t}{t_0} - 1\right)}}{c} \quad (2)$$

$$[\eta] = 3.5 \times 10^{-4} \times M_v^{\,0.57} \quad (3)$$

RESULTS AND DISCUSSION

Effect of Silica Nanofibers on the Sol−Gel Transition of Thermosensitive Polymers. The phase transitions of PNVCL and its nanocomposite aqueous solutions (1% m/v) were evaluated by the variation of their transmittance at different temperatures. PNVCL is found as a soluble transparent aqueous solution at room temperature; however, it becomes opaque with its phase transition, exhibiting a cloud point temperature (T_{cp}, 34 °C). The drop in the transmittance of PNVCL suspension is due to the formation of aggregates of polymer chains, as shown in our previous study.[11] In the presence of 1 and 5 wt % silica nanofibers with an average length and diameter of 500 and 70 nm, respectively (Figure 1), the nanocomposites showed T_{cp} values similar to those of pure PNVCL, with a slight increase of 1 °C for PN-1% SiO_2 (Figure 2). These T_{cp} values could indicate the formation of polymer chains with similar molecular weights in the presence of silica nanofibers since differences in the molecular weight of PNVCL affect the T_{cp} value.[10,66] While PNVCL solution had a sharp drop of its transmittance in the temperature interval between 33 and 34 °C,[11] the transmittance of nanocomposite suspensions reduced gradually as the temperature increased from 25 to 35 °C. To the best of our knowledge, this phenomenon has never been observed previously in thermosensitive nanocomposite systems based on PNVCL[5,22] or even others, such as PNIPAm.[20,23,24] The diffuse reduction of the transmittance could be related to the network formed by

https://dx.doi.org/10.1021/acs.langmuir.0c03079
Langmuir 2021, 37, 1531−1541

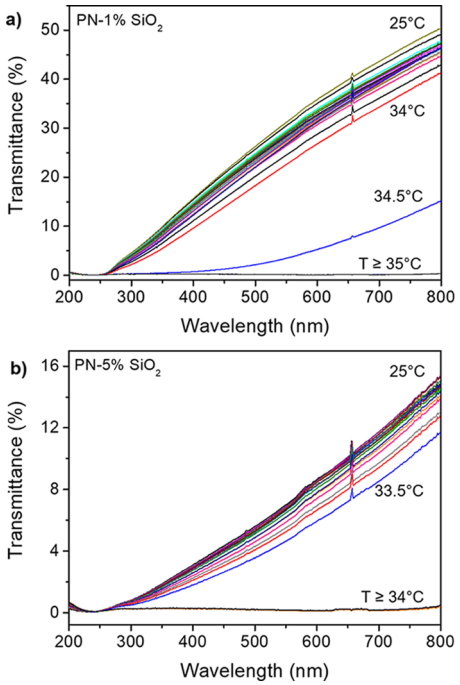

Figure 2. UV−vis spectra of 1% m/v aqueous nanocomposite dispersions of PNVCL with 1% (a) and 5% (b) silica nanofibers, from 25 to 40 °C (0.5 °C steps).

PNVCL and silica, changing the self-agglomeration profile of the polymer chains imposed by the presence of the nanofibers.

It was also observed that with the increasing amount of silica in the nanocomposites, the transmittance at 25 °C gets lower, obtaining at the 800 nm wavelength, the percent transmittance values of 50% for PN-1% SiO_2 and 15% for PN-5% SiO_2. Aiming to identify if this initial lower transmittance of nanocomposites is an effect of the intrinsic turbidity of silica, Figure S1 presents the transmittance profile solely of the silica nanofiber colloidal suspensions at the theoretical concentrations (1 and 5%) found in the nanocomposites, considering the dilution factor used (1% m/v) for the UV−vis analyses. The transmittance values of the silica suspensions at concentrations of 1 and 5% in the wavelength of 800 nm were 85 and 44%, respectively, which are higher than the ones found for the nanocomposites. While the transmittance intensity varies similarly for both silica dispersions in the analyzed wavelength range, the transmittance intensity of the nanocomposites varied according to the sample, the concentration of silica, and the wavelength. In this way, the distinct turbidity of the nanocomposites observed in temperatures below the T_{cp} value is ascribed to the presence of silica along with the new macromolecular arrangements formed by the interaction of silica with PNVCL. These novel structures could have larger and heterogeneous scattering centers and states of solvation and/or colloidal stability, causing the transmittance reduction.

To investigate the effect of silica nanofibers in the thermodynamic parameters of the phase transition, only two states for the polymer chains were considered, solvated or globular states, in analogy with van't Hoff's analysis on the unfolding of globular proteins.[67−69] Following this model, Alf *et al.*,[68] Tiktopulo *et al.*,[69] and Fuciños *et al.*[70] calculated the enthalpy changes during the sol−gel transition of PNIPAm derivative systems. In a similar approach, we employed the mathematical model (eq 4) introduced by Fuciños *et al.*[70] to calculate the thermodynamic parameters of PNVCL and its nanocomposites from the UV−vis experimental data.

$$OD = OD_S - \frac{OD_G - OD_S}{1 + e^{-((T-T_m)(T_m \cdot \Delta C_p - \Delta H^{\circ}_m)/R \cdot T \cdot T_m)}(T/T_m)^{(\Delta C_p/R)}} \quad (4)$$

$$OD = 2 - \log(T\%) \quad (5)$$

ΔC_p is the molar heat capacity change, ΔH°_m is the enthalpy changes in the midpoint of the phase transition curve ($T = T_m$), R is the gas constant (8.314 J mol^{-1} K^{-1}), OD is the optical density obtained by eq 5, and T% is the transmittance of the material suspensions in an intermediate wavelength (*e.g.*, 500 nm) previously shown in Figure 2. The OD is related to the concentration of the components in the system, and when observed at different temperatures, it showed the transition from the initially solvated polymer chains to the collapsed state with globular conformation. OD values corresponding to the solvated (OD_S) and globular (OD_G) states are the points of the curves with the lowest and highest values. At any temperature (T) within the phase transition, the polymer chains coexist in both solvated and globular states by assuming a two-state equilibrium system.[67,70] In this condition, the partial agglomeration of the polymer in solution is mathematically equivalent to the coexistence of a fraction of solvated polymer chains in equilibrium with a globular fraction. When $T = T_m$, the polymer chains in the solvated and globular phases have the same concentration. With this assumption, the curves of OD with temperature for PNVCL and its nanocomposites were fitted by eq 4 in Figure 3, and the thermodynamic parameters were calculated, as shown in Table 1.

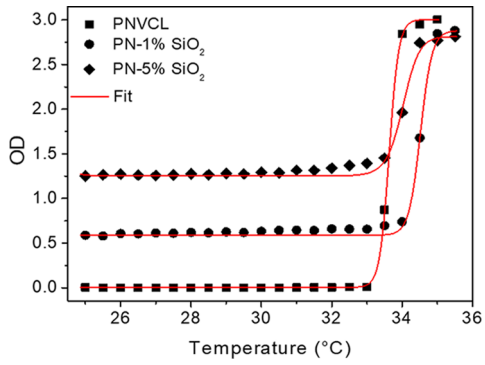

Figure 3. Optical density (OD) variation as a function of temperature (solid circles) of aqueous suspensions (1% w/v) of PNVCL and its nanocomposites with 1 and 5% silica nanofibers. The red lines are the fitting curves from eq 4.

PNVCL exhibits constant OD values until reaching the T_{cp} value, where there is an abrupt increase in OD values (Figure 3). The OD values of nanocomposites are slightly increasing with the heating until the systems undergo the phase transition and reach higher OD values. The observation of this slight increase in OD values below the T_{cp} value is not predicted by the mathematical model of eq 5. This phenomenon indicates that silica nanofibers introduced a third additional state to the solvated and globular states predicted for homopolymers and could be related to the interface generated from silica and

https://dx.doi.org/10.1021/acs.langmuir.0c03079
Langmuir 2021, 37, 1531−1541

Table 1. Cloud Point Temperature (T_{cp}), Solvated (OD_S) and Globular (OD_G) Optical Density Values Estimated by the UV−vis Spectra, T_m, and $\Delta H°_m$ Values Were Obtained by the Fitting of Eq 4 to the Optical Density as a Function of Temperature for PNVCL and its Nanocomposites with 1 and 5% Silica Nanofibers

material	T_{cp}, UV−vis (°C)	OD_S	OD_G	T_m (°C)	$\Delta H°_m$ (kJ mol^{-1})
PNVCL	34	0.005	3.003	33.63 ± 0.01	5789 ± 202
PN-1% SiO_2	35	0.589	2.880	34.52 ± 0.01	4784 ± 575
PN-5% SiO_2	34	1.251	2.812	34.02 ± 0.03	3346 ± 398

polymer interactions. Interestingly, the reported curves of PNIPAm-based polymer systems[68,70] demonstrated that the transition between the solvated and globular states occurred in a wider temperature range (~5 to 13 °C) than PNVCL (1 °C). Consequently, the transition region had a greater number of points (>6) than those obtained (1) for the PNVCL and its nanocomposites, highlighting another singularity of systems based on the PNVCL compared to PNIPAm systems, a sharp temperature-induced phase transition.

According to the fitting curves, the calculated T_m value agrees with previous T_{cp} values found in the transmittance spectra of Figure 2, demonstrating that the model in eq 4 was efficient for the prediction of T_{cp}. For the nanocomposites, the increase in silica nanofiber concentration resulted in lower values of $\Delta H°_m$, obtained in relation to the number of moles of cooperative units, which are the domains of the polymer chains involved in the sol−gel transition. This reduction may be related to what Alf *et al.*[68] found for cross-linked PNIPAm polymers. The formation of an interconnected nanostructured system of silica nanofibers and polymer chains reduced the mobility of the polymer, and the presence of silica added a steric hindrance to the solvation of polymer chains. Thus, this system presented a smaller cooperative unit, reducing the enthalpic contribution per monomeric unit.

In this way, the thermodynamic parameters indicated the formation of a network of polymer chains and silica nanofibers with reduced mobility. Nevertheless, the presence of silica nanofibers in nanocomposites may affect the local molecular motions of PNVCL chains, especially the groups directly bonded to the nanofibers. Additionally, the hydration of polymer chains and the process of temperature-induced phase transition will be influenced by the presence of a second component in the coil and globule phases. The network created by the interaction of polymer and silica nanofibers will vary the spin−lattice and spin−spin relaxation in NMR analysis and change with temperature. With this analysis, it is possible to deduce the intermolecular motions during the sol−gel transition of nanocomposites based on thermosensitive polymers.

Effect of Silica Nanofibers in the Macromolecular Motions of PNVCL-Based Nanocomposites by NMR Spectroscopy. Figure 4a shows high-resolution ^{1}H NMR (400 MHz) spectra of PNVCL in D_2O (5% m/v) measured at different temperatures (from 25 to 40 °C) under the same instrumental conditions. These spectra show four protons with resonance assignments in 4.14 ppm (br, 1H), 3.11 ppm (br, 2H), 2.25 ppm (br, 2H), and 1.59 ppm (br, 8H). Under heating, the intensity of PNVCL signals gradually decreased.

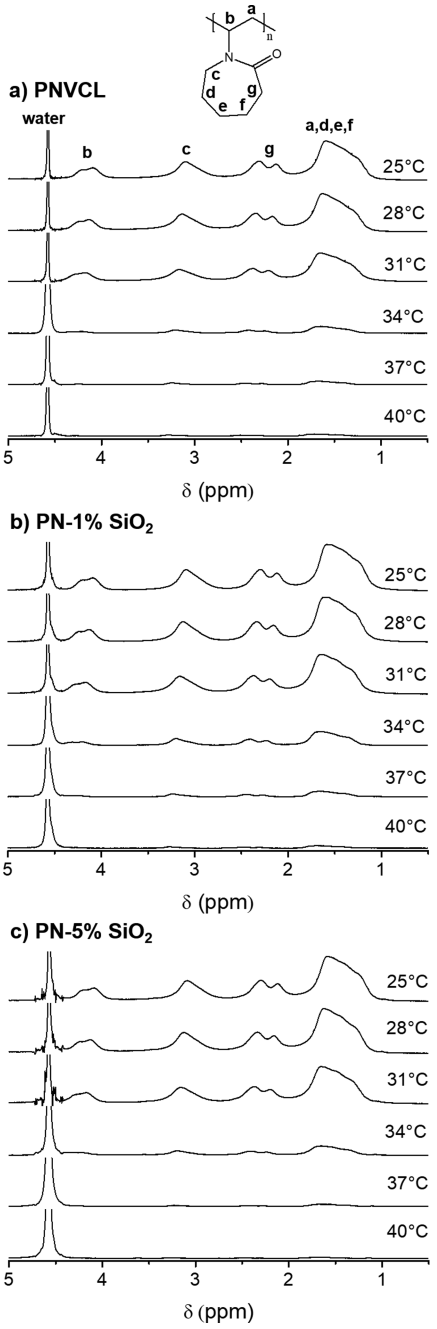

Figure 4. ^{1}H NMR (400 MHz) spectra of PNVCL (a), PN-1% SiO_2 (b), and PN-5% SiO_2 (c) in D_2O (5% m/v) at different temperatures. Relaxation delay was 1.0 s, and 64k time domain points were acquired for a spectral window of 20 ppm, resulting in an acquisition time of 2.04 s. δ is the chemical shift.

Remarkably, the NMR signal reduction is clearly observed at 34 °C (T_{cp}), which main PNVCL resonance peaks became broad and difficult to be detected. This feature is due to the reduced mobility of thermosensitive polymer chains when transit from coil to globule states above the T_{cp} value.[31,46] PNVCL nanocomposites with 1 and 5% silica nanofibers presented similar spectra to PNVCL, as shown in Figure 4b,c, respectively, without additional peaks or evident chemical displacement of PNVCL resonance assignments. Similarly, the drop in intensity and enlargement of peaks were mainly observed above 34 °C.

https://dx.doi.org/10.1021/acs.langmuir.0c03079
Langmuir 2021, 37, 1531−1541

The reduction of integrated intensities of PNVCL and nanocomposite protons with temperature is better identified by following the integrated intensity of PNVCL methylene groups at 1.6 ppm in Figure 5. The integrated intensity in the

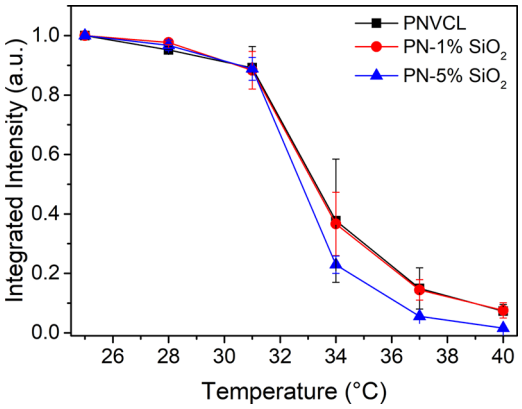

Figure 5. Normalized ^{1}H NMR integrated intensities of methylene groups in δ = 1.6 ppm PNVCL, PN-1% SiO_2, and PN-5% SiO_2 dispersed in D_2O (5% m/v) at different temperatures.

temperature range of 28−40 °C was normalized to the integrated intensity at 25 °C for each material. Although the T_{cp} value for the materials is in the range of 34−35 °C, the signal already reduced at 31 °C an average of 11% for PNVCL and its nanocomposites, possibly indicating the formation of an intermediate state where the polymer chains start to arrange into a more compact structure with reduced mobility.[36] Above the T_{cp} value, the signal intensity continued to reduce at 37 and 40 °C, which could be explained by the shrinking of physically cross-linked hydrogels at higher temperatures, resulting in a restrained macromolecular mobility.[36] Among the materials, PNVCL and PN-1% SiO_2 showed similar variations of the integrated intensities of methylene groups. Meanwhile, PN-5% SiO_2 showed the smallest intensity values above the T_{cp} value, acquiring a stronger motional restriction of the polymer segments in the nanocomposite network with higher silica content. Possible variations in the profile observed in the NMR data with previous turbidimetry measurements can be related to concentration differences in polymer/nanocomposite solutions, formation of small globules below the T_{cp} value that do not scatter light in the visible spectra but already have restrained mobility, and slightly differences in the hydrogen bonding interactions in the presence of D_2O.

PNVCL forms a transparent colloidal suspension of solvated polymer chains when dispersed in water.[71,72] When heated above the T_{cp} value, the polymer chains agglomerate by intermolecular interactions such as dipole−dipole interactions between polar amide groups and van der Waals forces between the major polymer chains and hydrogen bonds of C═O and water molecules trapped within the polymer globules.[65] Meanwhile, the nanocomposites have functionalized silica nanofibers, which methacrylate groups can react with the NVCL monomers via *in situ* polymerization and promote the covalent bonding between the inorganic and organic components.[73] The formation of an interconnected structure of silica and polymer chains may affect PNVCL intermolecular interactions during the temperature-induced phase transition as well as its interaction with water molecules. The process of hydration and dehydration of polymer chains and nanocomposite networks during the phase transition can be described by the decay of transverse magnetization (T_2) of normalized NMR signal integral of water proton (4.5 ppm) as a function of spin-echo time (τ) at different temperatures, as shown in Figure S2. When water molecules with different dynamics are found, it is possible to reveal the complex process of association and dissociation of thermosensitive nanocomposites in aqueous media below T_{cp}, at T_{cp}, and above this temperature. Depending on the evaluated temperature of polymer/nanocomposite systems, biexponential functions for the T_2 decay give the best fit. This biexponential profile from the transverse magnetization indicates the heterogeneity of molecular dynamics, as demonstrated in core−corona structures and other thermosensitive polymers.[2,30,34]

The T_2 values calculated from the exponential function are shown in Table 2. For PNVCL, a biexponential profile of

Table 2. Short (T_{2S}) and Long (T_{2L}) Components for the Water Proton Transverse Relaxation Times (s) Calculated from the Exponential Decay for PNVCL, PN-1% SiO_2, and PN-5% SiO_2 at Different Temperatures

	PNVCL		PN-1% SiO_2		PN-5% SiO_2	
temperature (°C)	T_{2S}	T_{2L}	T_{2S}	T_{2L}	T_{2S}	T_{2L}
25		4.13		3.48		1.59
28		3.97		3.41		1.69
31		3.84		3.38		1.58
34	0.27	3.84		3.92		0.74
37	0.07	3.53		2.68		0.84
40	0.11	3.56	0.97	2.56		1.13

relaxation curves observed at temperatures above 34 °C generated two T_2 values. A short transverse relaxation value is related to water molecules with restricted mobility, while a long transverse relaxation value corresponds to the highly mobile portion, as free water molecules.[32,45] Below the T_{cp} value, PNVCL has a random coil structure in the aqueous solution, where free water and water molecules interacting with hydrophilic polymer groups by hydrogen bonds are present. Once the PNVCL system reached the T_{cp} value at 34 °C, polymer chain moieties agglomerated into the globule phase, revealing a second short T_2 value (T_{2S}). This second T_2 value arose from water molecules trapped in polymer globules with spatially restricted mobility, which are still present in higher temperatures for PNVCL systems.[32,46] Kametani *et al.*[32] and Watanabe *et al.*[31] also observed two or even more T_2 values for water molecules with different dynamics due to the presence of heterogeneities of the thermosensitive polymer systems such as poly(*N*-isopropylacrylamide) and polypoly(asparagine) derivative, respectively.

Meanwhile, the nanocomposites presented a single-exponential profile for the transverse magnetization for most evaluated temperatures, indicating a fast exchange among free water and water molecules interacting with PNVCL.[46] Only at 40 °C, a second short T_2 value is revealed for PN-1% SiO_2, indicating a portion of water molecules with restricted motion in the gel state. Then, at first glance, the presence of silica nanofibers changed the water dynamics above the T_{cp} value. They could compromise the absorption of water molecules into the globule phase, also influenced by the hydrophobic character of functionalized nanofibers interconnected with polymer chains. Comparing the variation of T_{2L} with temperature for PNVCL and its nanocomposites in Figure 6, the presence of silica changed the water dynamics by reducing

https://dx.doi.org/10.1021/acs.langmuir.0c03079
Langmuir 2021, 37, 1531−1541

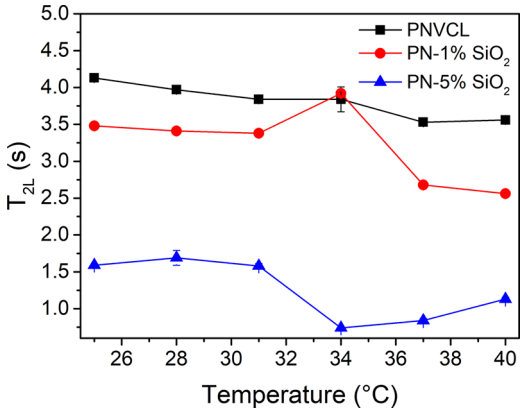

Figure 6. Variation of T_{2L} with temperature of water molecules for PNVCL and its nanocomposites. Lines were drawn to guide the eye.

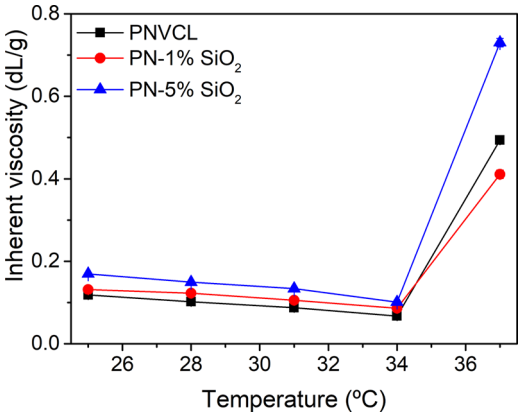

Figure 7. Inherent viscosity of PNVCL and its nanocomposite solutions (1% m/v) at different temperatures.

the overall T_{2L} value due to mobility reduction. Meanwhile, the T_2 value of pure water increases linearly with temperature, and below the T_{cp} value, the T_{2L} values slightly changed according to motional restrictions of water molecules binding to PNVCL chains.[36] In the temperature-induced phase transition, the formation of a network of physically cross-linked polymer chains confined water molecules in a globular state, resulting in a similar T_{2L} value and an emergence of a short T_2 value. Above the T_{cp} value, the globules are further compacting and releasing water, which mobility is still lightly restricted due to its binding to the outer part of globules.[36] Additionally, the water molecules mainly exist as free bulk water, presenting similar or slightly increasing mobility with temperature.[30,32]

PN-1% SiO_2 showed a higher T_{2L} value at 34 °C since this temperature is below its T_{cp} and the mobility of water can increase with temperature before reaching the T_{cp} value at 35 °C and acquire a restricted mobility.[30] However, T_{2L} values reduced at 37 and 40 °C, indicating that the presence of water molecules with confined mobility probably absorbed in the collapsed state of this nanocomposite. PN-5% SiO_2 had a similar T_{2L} value drop to PNVCL at 34 °C, and its T_{2L} values slightly increased at 37 and 40 °C. According to the profile of T_{2L} value variation with the temperature, the imprisonment and release of water molecules resulting from the coil−globule transition of nanocomposites happened in a wider temperature range compared to pure PNVCL. This behavior could be related to the gradual transmittance reduction with increasing temperature, previously shown in Figure 2.

Although it is reported that the NMR relaxation times can be independent on polymer chemical structure, molar mass, and variation of bulk viscosity in polymer solutions with a concentration up to 5−10 wt %, we investigated the inherent viscosity of PNVCL and nanocomposite systems (1% m/v) in different temperatures. Figure 7 shows an increase in inherent viscosity for the nanocomposites, indicating an additional of approximately 20% for PN-1% SiO_2 and 47% PN-5% SiO_2 in the viscosity of PNVCL. The viscosity of all systems slightly decreased with temperature until surpassed the T_{cp} value, where an abrupt increase in inherent viscosity indicated the formation of the gel state. By using the viscosity values found at 25 °C, it was possible to calculate the viscosity average molecular weights (M_v) of the systems shown in Table S1. The increasing amount of silica nanofibers contributed to obtain PNVCL with higher molecular weight. This increase can be ascribed to the polymerization process of the methacrylate groups from silica nanofibers with NVCL monomers, resulting in polymer chains connected by silica nanofibers.[74] Based on this result, the presence of silica nanofibers interconnected with the PNVCL chains could restrict the chain motion, the intermolecular interaction, and entanglements during the phase transition as well as vary the relaxation time of water molecules absorbed in the nanocomposite systems. However, the difference of molecular weight among the three samples is not expected to influence the relaxation times measured in the present study since T_2 and T_1 are usually independent of polymer molecular weight at concentrations below 100 mg mL^{-1}.[75]

Aiming to investigate in more details how the interaction of PNVCL and inorganic nanoparticles affected the sol−gel transition of thermosensitive polymer systems, the spin−lattice relaxation time (T_1) of each proton from the four PNVCL resonance assignments was investigated at the temperature range of 25−40 °C. By the decay of longitudinal magnetization of normalized NMR signal integral of the protons as a function of time interval between 180 and 90° pulses in the inversion recovery experiment, it was possible to determine the T_1 values for each site of the polymer structure highlighted in Figure 8a. By fitting a single-exponential profile (present in Figures S3, S4, and S5), T_1 values for all polymer regions, temperatures, and samples were determined, as shown in Figure 8.

T_1 values remarkably changed for PNVCL and nanocomposites with 1 and 5% silica nanofibers. They showed a distinct profile within the temperature range and were dependent on the analyzed proton, which indicates specific segmental motions and intramolecular interactions of the polymer regions analyzed. Although T_1 and T_2 can have similar values in lower correlation times and mobile solutions, they can differ in viscous solutions and higher correlation times. In this case, T_1 goes through a minimum and T_2 decreases with correlation time as proposed by Bloembergen−Purcell−Pound theory.[30,76,77] This same profile can be observed when a polymer solution is investigated in a range of temperatures,[75,78] and it was clearly observed in Figure 8b for PNVCL. In addition to the temperature effect, the variation of T_1 for proton b of PNVCL also reflects the contribution of the coil−globule transition, reducing the polymer mobility. It corroborates with the previous result of Figure 4, in which a less mobile intermediate state with less intense NMR signals of the polymers is formed at 31 °C.

https://dx.doi.org/10.1021/acs.langmuir.0c03079
Langmuir 2021, 37, 1531−1541

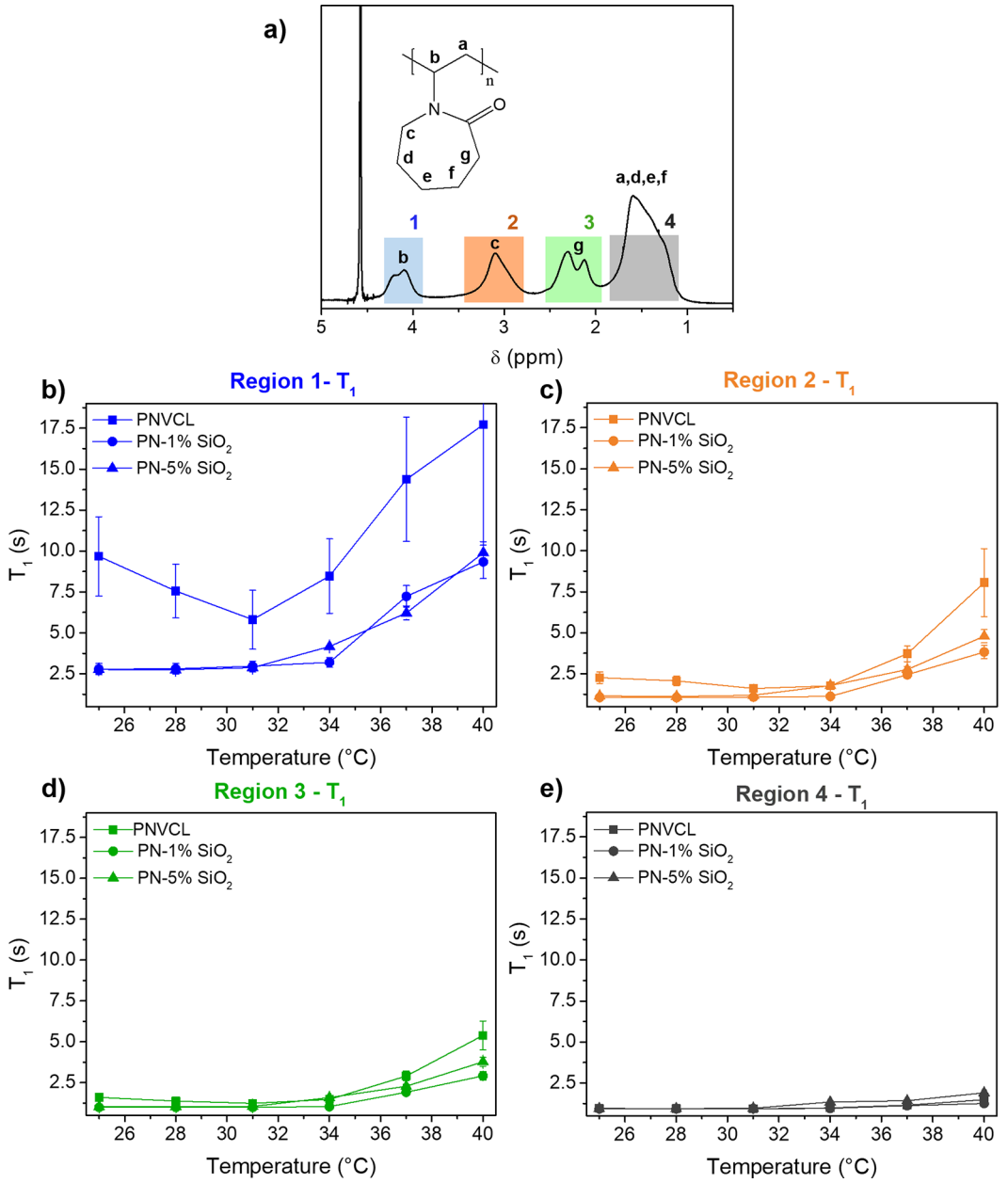

Figure 8. Variation of the spin−lattice relaxation time (T_1) calculated for the four proton resonances (a) described as regions 1 (b), 2 (c), 3 (d), and 4 (e) of PNVCL, PN-1% SiO_2, and PN-5% SiO_2.

The neighbor protons of the lactam group (b, c, and g) in Figure 8b−d, respectively, from the nanocomposites are more susceptible to mobility changes due to a possible interaction with SiO_2 nanofibers. Additionally, the silica has a hydrophobic behavior associated to the MPS functional groups attached to the mesopores, as shown in the thermogravimetric analysis in Figure S6, limiting the surrounding interaction with water. The combination of these two factors can contribute to hinder the interaction with water molecules through the entire extension of polymer chains and the water molecule imprisonment in the globule state above the T_{cp} value. As a consequence, smaller variations of T_1 values of protons b, c, and g in the agglomerated and swollen states are observed for the nanocomposites when compared to neat PNVCL. While the proton b has a variation of ΔT_1 between 40 and 25 °C of 8 s, PN-1% SiO_2 and PN-5% SiO_2 showed smaller variations of 6.5 and 7.1 s, respectively. The same trend was observed for protons c and g, whose ΔT_1 underwent a reduction of 52% (proton c) and 50% (proton g) for PN-1% SiO_2 and 38% (proton c) and 29% (proton g) for PN-5% SiO_2 when compared to ΔT_1 for PNVCL. These results corroborate to the previous T_{2S} value observed for PNVCL and related to the trapped water molecules in the polymer globules above the T_{cp} value, which were not observed in the nanocomposites.

On the other hand, protons a, d, e, and f in region 4 (Figure 8e) have similar mobility and less influence of the presence of silica nanofibers and from the phase transition. The similar T_1 values obtained for PNVCL and nanocomposites indicate the poor interaction of these protons with the silica and water molecules. Thereby, the presence of nanoparticles bound to thermosensitive polymers can remarkably change the phase transition and the macromolecular arrangements. Although PNVCL and its nanocomposites showed similar T_{cp} values by turbidity measurements, the silica nanofibers restrained the

https://dx.doi.org/10.1021/acs.langmuir.0c03079
Langmuir 2021, 37, 1531−1541

overall polymer backbone mobility. Notably, they changed the intermolecular and intramolecular interactions as well as the water solvation, especially in the surrounding of the lactam group during the coil−globule transition. While the protons b, c, and g experienced changes imposed by the silica nanofibers, protons c and g had larger modification when compared to pure PNVCL. This result is an indication that the inter- and intramolecular interactions of the lactam groups are the main polymer segments involved in the aggregation and formation of the globular state in PNVCL instead of the backbone chains.

CONCLUSIONS

In this study, a singular strategy to investigate multifunctional nanocomposite hydrogels was proposed since traditional techniques might not be effective to study systems with stimuli-sensitive properties. Nanocomposites of PNVCL and mesoporous silica nanofibers have great potential as a smart drug delivery platform according to their thermosensitive properties, biocompatibility, and ability to immobilize different components into their mesopores. However, in order to tailor the nanocomposite properties and applications, the physicochemical aspects and structural changes under stimuli were needed to be investigated. The presence of silica nanofibers remarkably changed the polymer motions in aqueous media. T_1 and T_2 relaxation times revealed that the nanocomposites had restrained mobility compared to neat PNVCL, and the phase transition was influenced mainly by the inter- and intramolecular interactions of neighbor bonds of the lactam group, instead of just the polymer backbone immobilized by the silica nanofibers. The gradual transmittance changes of nanocomposites with the temperature indicated the formation of additional intermediate components to the coil−globule states in the phase transition, with also a wider temperature range for the hydration/dehydration process. These features open up opportunities to develop and understand hierarchical nanocomposites with tunable and sensitive properties to small temperatures and environmental variations. In particular, the proposed materials and characterization methodology can find potential use in the development of drug delivery systems to perform on-demand pulsatile release of different drugs.

ASSOCIATED CONTENT

Supporting Information

The Supporting Information is available free of charge at https://pubs.acs.org/doi/10.1021/acs.langmuir.0c03079.

UV−vis spectra of silica nanofiber colloidal dispersions, thermogravimetric analysis of functionalized silica nanofibers, table of viscosity average molecular weights of PNVCL and its nanocomposites, and ^{1}H NMR transverse and longitudinal relaxation decays with exponential fit for PNVCL and its nanocomposites with 1 and 5% silica nanofibers (PDF)

AUTHOR INFORMATION

Corresponding Authors

Renata L. Sala − *Department of Chemistry, Federal University of São Carlos (UFSCar), São Carlos, SP 13565-905, Brazil;* orcid.org/0000-0001-5446-5346; Email: renata.lang89@gmail.com

Emerson R. Camargo − *Department of Chemistry, Federal University of São Carlos (UFSCar), São Carlos, SP 13565-905, Brazil*; Email: camargo@ufscar.br

Author

Tiago Venâncio − *Department of Chemistry, Federal University of São Carlos (UFSCar), São Carlos, SP 13565-905, Brazil;* orcid.org/0000-0002-5592-3940

Complete contact information is available at: https://pubs.acs.org/10.1021/acs.langmuir.0c03079

Author Contributions

All authors have given approval to the final version of the manuscript.

Notes

The authors declare no competing financial interest.

ACKNOWLEDGMENTS

This study was financed in part by the Coordenação de Aperfeiçoamento de Pessoal de Nível Superior - Brasil (CAPES) - Finance Code 001, Conselho Nacional de Desenvolvimento Científico e Tecnológico (CNPq) and São Paulo Research Foundation (FAPESP) grants #2013/25663-2, #2015/13958-3, and #2013/07296-2 (CEPID/CDMF). We thank Prof. Edson R. Leite and Prof. Elson Longo for access to characterization facilities. We thank Prof. Sandra A. Cruz, Prof. Caio M. Paranhos, and Leticia Akemi for their valuable assistance in the viscosity measurements.

REFERENCES

(1) Stuart, M. A. C.; Huck, W. T. S.; Genzer, J.; Müller, M.; Ober, C.; Stamm, M.; Sukhorukov, G. B.; Szleifer, I.; Tsukruk, V. V.; Urban, M.; Winnik, F.; Zauscher, S.; Luzinov, I.; Minko, S. Emerging applications of stimuli-responsive polymer materials. *Nat. Mater.* **2010**, *9*, 101−113.

(2) Etchenausia, L.; Deniau, E.; Brûlet, A.; Forcada, J.; Save, M. Cationic Thermoresponsive Poly(*N*-vinylcaprolactam) Microgels Synthesized by Emulsion Polymerization Using a Reactive Cationic Macro-RAFT Agent. *Macromolecules* **2018**, *51*, 2551−2563.

(3) Nguyen, Q. V.; Huynh, D. P.; Park, J. H.; Lee, D. S. Injectable polymeric hydrogels for the delivery of therapeutic agents: A review. *Eur. Polym. J.* **2015**, *72*, 602−619.

(4) Dutta, K.; De, S. Smart responsive materials for water purification: an overview. *J. Mater. Chem. A* **2017**, *5*, 22095−22112.

(5) Chang, B.; Chen, D.; Wang, Y.; Chen, Y.; Jiao, Y.; Sha, X.; Yang, W. Bioresponsive Controlled Drug Release Based on Mesoporous Silica Nanoparticles Coated with Reductively Sheddable Polymer Shell. *Chem. Mater.* **2013**, *25*, 574−585.

(6) Vihola, H.; Laukkanen, A.; Hirvonen, J.; Tenhu, H. Binding and release of drugs into and from thermosensitive poly(*N*-vinyl caprolactam) nanoparticles. *Eur. J. Pharm. Sci.* **2002**, *16*, 69−74.

(7) Donova, M. V.; Kuzkina, I. F.; Arinbasarova, A. Y.; Pashkin, I. I.; Markvicheva, E. A.; Baklashova, T. G.; Sukhodolskaya, G. V.; Fokina, V. V.; Kirsh, Y. E.; Koshcheyenko, K. A.; Zubov, V. P. Poly-N-vinylcaprolactam gel: A novel matrix for entrapment of microorganisms. *Biotechnol. Tech.* **1993**, *7*, 415−422.

(8) Markvicheva, E. A.; Tkachuk, N. E.; Kuptsova, S. V.; Dugina, T. N.; Strukova, S. M.; Kirssh, Y. E.; Zubov, V. P.; Rumish, L. D. Stabilization of proteases by entrapment in a new composite hydrogel. *Appl. Biochem. Biotechnol.* **1996**, *61*, 75−84.

(9) Lynch, B.; Crawford, K.; Baruti, O.; Abdulahad, A.; Webster, M.; Puetzer, J.; Ryu, C.; Bonassar, L. J.; Mendenhall, J. The effect of hypoxia on thermosensitive poly(N-vinylcaprolactam) hydrogels with tunable mechanical integrity for cartilage tissue engineering. *J. Biomed. Mater. Res., Part B* **2017**, *105*, 1863−1873.

(10) Sala, R. L.; Kwon, M. Y.; Kim, M.; Gullbrand, S. E.; Henning, E. A.; Mauck, R. L.; Camargo, E. R.; Burdick, J. A. Thermosensitive Poly(N-vinylcaprolactam) Injectable Hydrogels for Cartilage Tissue Engineering. *Tissue Eng., Part A* **2017**, *23*, 935−945.

(11) Sala, R. L.; Gonçalves, R. H.; Camargo, E. R.; Leite, E. R. Thermosensitive poly(N-vinylcaprolactam) as a transmission light regulator in smart windows. *Sol. Energy Mater. Sol. Cells* **2018**, *186*, 266−272.
(12) Merino, S.; Martín, C.; Kostarelos, K.; Prato, M.; Vázquez, E. Nanocomposite Hydrogels: 3D Polymer−Nanoparticle Synergies for On-Demand Drug Delivery. *ACS Nano* **2015**, *9*, 4686−4697.
(13) Vashist, A.; Vashist, A.; Gupta, Y. K.; Ahmad, S. Recent advances in hydrogel based drug delivery systems for the human body. *J. Mater. Chem. B* **2014**, *2*, 147−166.
(14) Siegel, R. A. Stimuli sensitive polymers and self regulated drug delivery systems: A very partial review. *J. Controlled Release* **2014**, *190*, 337−351.
(15) Gaharwar, A. K.; Peppas, N. A.; Khademhosseini, A. Nanocomposite hydrogels for biomedical applications. *Biotechnol. Bioeng.* **2014**, *111*, 441−453.
(16) Yan, B.; Boyer, J.-C.; Habault, D.; Branda, N. R.; Zhao, Y. Near Infrared Light Triggered Release of Biomacromolecules from Hydrogels Loaded with Upconversion Nanoparticles. *J. Am. Chem. Soc.* **2012**, *134*, 16558−16561.
(17) Strong, L. E.; Dahotre, S. N.; West, J. L. Hydrogel-nanoparticle composites for optically modulated cancer therapeutic delivery. *J. Controlled Release* **2014**, *178*, 63−68.
(18) Nagahama, K.; Kawano, D.; Oyama, N.; Takemoto, A.; Kumano, T.; Kawakami, J. Self-Assembling Polymer Micelle/Clay Nanodisk/Doxorubicin Hybrid Injectable Gels for Safe and Efficient Focal Treatment of Cancer. *Biomacromolecules* **2015**, *16*, 880−889.
(19) Koshy, S. T.; Zhang, D. K. Y.; Grolman, J. M.; Stafford, A. G.; Mooney, D. J. Injectable nanocomposite cryogels for versatile protein drug delivery. *Acta Biomater.* **2018**, *65*, 36−43.
(20) Park, J.-H.; Lee, Y.-H.; Oh, S.-G. Preparation of Thermosensitive PNIPAm-Grafted Mesoporous Silica Particles. *Macromol. Chem. Phys.* **2007**, *208*, 2419−2427.
(21) Loos, W.; Verbrugghe, S.; Goethals, E. J.; Du Prez, F. E.; Bakeeva, I. V.; Zubov, V. P. Thermo-Responsive Organic/Inorganic Hybrid Hydrogels based on Poly(N-vinylcaprolactam). *Macromol. Chem. Phys.* **2003**, *204*, 98−103.
(22) Karesoja, M.; McKee, J.; Karjalainen, E.; Hietala, S.; Bergman, L.; Linden, M.; Tenhu, H. Mesoporous silica particles grafted with poly(ethyleneoxide-*block*-*N*-vinylcaprolactam). *J. Polym. Sci., Part A: Polym. Chem.* **2013**, *51*, 5012−5020.
(23) Li, M.; Song, X.; Zhang, T.; Zeng, L.; Xing, J. Aggregation induced emission controlled by a temperature-sensitive organic-inorganic hybrid polymer with a particular LCST. *RSC Adv.* **2016**, *6*, 86012−86018.
(24) Chung, P.-W.; Kumar, R.; Pruski, M.; Lin, V. S.-Y. Temperature Responsive Solution Partition of Organic−Inorganic Hybrid Poly(*N*-isopropylacrylamide)-Coated Mesoporous Silica Nanospheres. *Adv. Funct. Mater.* **2008**, *18*, 1390−1398.
(25) Ndoro, T. V. M.; Böhm, M. C.; Müller-Plathe, F. Interface and Interphase Dynamics of Polystyrene Chains near Grafted and Ungrafted Silica Nanoparticles. *Macromolecules* **2012**, *45*, 171−179.
(26) Buryachenko, V. A.; Roy, A.; Lafdi, K.; Anderson, K. L.; Chellapilla, S. Multi-scale mechanics of nanocomposites including interface: Experimental and numerical investigation. *Compos. Sci. Technol.* **2005**, *65*, 2435−2465.
(27) Bedrov, D.; Smith, G. D.; Smith, J. S. Matrix-induced nanoparticle interactions in a polymer melt: A molecular dynamics simulation study. *J. Chem. Phys.* **2003**, *119*, 10438−10447.
(28) Song, Y.; Zheng, Q. Concepts and conflicts in nanoparticles reinforcement to polymers beyond hydrodynamics. *Prog. Mater. Sci.* **2016**, *84*, 1−58.
(29) Jancar, J.; Douglas, J. F.; Starr, F. W.; Kumar, S. K.; Cassagnau, P.; Lesser, A. J.; Sternstein, S. S.; Buehler, M. J. Current issues in research on structure−property relationships in polymer nanocomposites. *Polymer* **2010**, *51*, 3321−3343.
(30) Ohta, H.; Ando, I.; Fujishige, S.; Kubota, K. Molecular motion and 1H NMR relaxation of aqueous poly(N-isopropylacrylamide) solution under high pressure. *J. Polym. Sci., Part B: Polym. Phys.* **1991**, *29*, 963−968.
(31) Watanabe, E.; Boutis, G. S.; Sato, H.; Sekine, S.; Asakura, T. NMR studies of thermo-responsive behavior of an amphiphilic poly(asparagine) derivative in water. *Polymer* **2014**, *55*, 278−286.
(32) Kametani, S.; Sekine, S.; Ohkubo, T.; Hirano, T.; Ute, K.; Cheng, H. N.; Asakura, T. NMR studies of water dynamics during sol-to-gel transition of poly (N-isopropylacrylamide) in concentrated aqueous solution. *Polymer* **2017**, *109*, 287−296.
(33) Wada, H.; Kitazawa, Y.; Kuroki, S.; Tezuka, Y.; Yamamoto, T. NMR Relaxometry for the Thermal Stability and Phase Transition Mechanism of Flower-like Micelles from Linear and Cyclic Amphiphilic Block Copolymers. *Langmuir* **2015**, *31*, 8739−8744.
(34) Balaceanu, A.; Demco, D. E.; Möller, M.; Pich, A. Microgel Heterogeneous Morphology Reflected in Temperature-Induced Volume Transition and ^{1}H High-Resolution Transverse Relaxation NMR. The Case of Poly(*N*-vinylcaprolactam) Microgel. *Macromolecules* **2011**, *44*, 2161−2169.
(35) Willems, C.; Pargen, S.; Balaceanu, A.; Keul, H.; Möller, M.; Pich, A. Stimuli responsive microgels decorated with oligoglycidol macromonomers: Synthesis, characterization and properties in aqueous solution. *Polymer* **2018**, *141*, 21−33.
(36) Rusu, M.; Wohlrab, S.; Kuckling, D.; Möhwald, H.; Schönhoff, M. Coil-to-Globule Transition of PNIPAM Graft Copolymers with Charged Side Chains: A ^{1}H and ^{2}H NMR and Spin Relaxation Study. *Macromolecules* **2006**, *39*, 7358−7363.
(37) Phua, D. I.; Herman, K.; Balaceanu, A.; Zakrevski, J.; Pich, A. Reversible Size Modulation of Aqueous Microgels via Orthogonal or Combined Application of Thermo- and Phototriggers. *Langmuir* **2016**, *32*, 3867−3879.
(38) Melle, A.; Balaceanu, A.; Kather, M.; Wu, Y.; Gau, E.; Sun, W.; Huang, X.; Shi, X.; Karperien, M.; Pich, A. Stimuli-responsive poly(*N*-vinylcaprolactam-*co*-2-methoxyethyl acrylate) core−shell microgels: facile synthesis, modulation of surface properties and controlled internalisation into cells. *J. Mater. Chem. B* **2016**, *4*, 5127−5137.
(39) Rice, C. V. Phase-Transition Thermodynamics of *N*-Isopropylacrylamide Hydrogels. *Biomacromolecules* **2006**, *7*, 2923−2925.
(40) Chakraborty, I.; Mukherjee, K.; De, P.; Bhattacharyya, R. Monitoring Coil−Globule Transitions of Thermoresponsive Polymers by Using NMR Solvent Relaxation. *J. Phys. Chem. B* **2018**, *122*, 6094−6100.
(41) Starovoytova, L.; Spěváček, J. Effect of time on the hydration and temperature-induced phase separation in aqueous polymer solutions. ^{1}H NMR study. *Polymer* **2006**, *47*, 7329−7334.
(42) Starovoytova, L.; Spěváček, J.; Trchová, M. ^{1}H NMR and IR study of temperature-induced phase transition of negatively charged poly(*N*-isopropylmethacrylamide-*co*-sodium methacrylate) copolymers in aqueous solutions. *Eur. Polym. J.* **2007**, *43*, 5001−5009.
(43) Mukherji, D.; Wagner, M.; Watson, M. D.; Winzen, S.; de Oliveira, T. E.; Marques, C. M.; Kremer, K. Relating side chain organization of PNIPAm with its conformation in aqueous methanol. *Soft Matter* **2016**, *12*, 7995−8003.
(44) Spěváček, J. NMR investigations of phase transition in aqueous polymer solutions and gels. *Curr. Opin. Colloid Interface Sci.* **2009**, *14*, 184−191.
(45) Spěváček, J. NMR Investigations of Temperature-Induced Phase Transition in Aqueous Polymer Solutions. *Macromol. Symp.* **2011**, *305*, 18−25.
(46) Spěváček, J.; Dybal, J.; Starovoytova, L.; Zhigunov, A.; Sedláková, Z. Temperature-induced phase separation and hydration in poly(*N*-vinylcaprolactam) aqueous solutions: a study by NMR and IR spectroscopy, SAXS, and quantum-chemical calculations. *Soft Matter* **2012**, *8*, 6110−6119.
(47) Kimmich, R.; Fatkullin, N. Self-diffusion studies by intra- and inter-molecular spin-lattice relaxometry using field-cycling: Liquids, plastic crystals, porous media, and polymer segments. *Prog. Nucl. Magn. Reson. Spectrosc.* **2017**, *101*, 18−50.

https://dx.doi.org/10.1021/acs.langmuir.0c03079
Langmuir 2021, 37, 1531−1541

(48) Balasubramaniam, S.; Pothayee, N.; Lin, Y.; House, M.; Woodward, R. C.; St. Pierre, T. G.; Davis, R. M.; Riffle, J. S. Poly(*N*-isopropylacrylamide)-Coated Superparamagnetic Iron Oxide Nanoparticles: Relaxometric and Fluorescence Behavior Correlate to Temperature-Dependent Aggregation. *Chem. Mater.* **2011**, *23*, 3348−3356.
(49) Schweizerhof, S.; Demco, D. E.; Mourran, A.; Keul, H.; Fechete, R.; Möller, M. Temperature-Induced Phase Transition Characterization of Responsive Polymer Brushes Grafted onto Nanoparticles. *Macromol. Chem. Phys.* **2017**, *218*, 1600495.
(50) Zhou, J.; Wang, M.; Han, Y.; Lai, J.; Chen, J. Multistage-Targeted Gold/Mesoporous Silica Nanocomposite Hydrogel as In Situ Injectable Drug Release System for Chemophotothermal Synergistic Cancer Therapy. *ACS Appl. Bio Mater.* **2019**, *3*, 421−431.
(51) Gangrade, A.; Gawali, B.; Jadi, P. K.; Naidu, V. G. M.; Mandal, B. B. Photo-Electro Active Nanocomposite Silk Hydrogel for Spatiotemporal Controlled Release of Chemotherapeutics: An In Vivo Approach toward Suppressing Solid Tumor Growth. *ACS Appl. Mater. Interfaces* **2020**, *12*, 27905−27916.
(52) Mertz, D.; Harlepp, S.; Goetz, J.; Bégin, D.; Schlatter, G.; Bégin-Colin, S.; Hébraud, A. Nanocomposite Polymer Scaffolds Responding under External Stimuli for Drug Delivery and Tissue Engineering Applications. *Adv. Ther.* **2020**, *3*, 1900143.
(53) Rosales, A. M.; Anseth, K. S. The design of reversible hydrogels to capture extracellular matrix dynamics. *Nat. Rev. Mater.* **2016**, *1*, 15012.
(54) Rambaud, F.; Vallé, K.; Thibaud, S.; Julián-López, B.; Sanchez, C. One-Pot Synthesis of Functional Helicoidal Hybrid Organic-Inorganic Nanofibers with Periodically Organized Mesoporosity. *Adv. Funct. Mater.* **2009**, *19*, 2896−2905.
(55) Buchtová, N.; Réthoré, G.; Boyer, C.; Guicheux, J.; Rambaud, F.; Vallé, K.; Belleville, P.; Sanchez, C.; Chauvet, O.; Weiss, P.; le Bideau, J. Nanocomposite hydrogels for cartilage tissue engineering: mesoporous silica nanofibers interlinked with siloxane derived polysaccharide. *J. Mater. Sci.: Mater. Med.* **2013**, *24*, 1875−1884.
(56) Wang, S. Ordered mesoporous materials for drug delivery. *Microporous Mesoporous Mater.* **2009**, *117*, 1−9.
(57) Zou, H.; Wu, S.; Shen, J. Polymer/Silica Nanocomposites: Preparation, Characterization, Properties, and Applications. *Chem. Rev.* **2008**, *108*, 3893−3957.
(58) Abdelhamid, M. A. A.; Pack, S. P. Biomimetic and bioinspired silicifications: Recent advances for biomaterial design and applications. *Acta Biomater.* **2021**, *120*, 38−56.
(59) Buchtová, N.; D'Orlando, A.; Judeinstein, P.; Chauvet, O.; Weiss, P.; Le Bideau, J. Water dynamics in silanized hydroxypropyl methylcellulose based hydrogels designed for tissue engineering. *Carbohydr. Polym.* **2018**, *202*, 404−408.
(60) Ravichandran, R.; Gandhi, S.; Sundaramurthi, D.; Sethuraman, S.; Krishnan, U. M. Hierarchical mesoporous silica nanofibers as multifunctional scaffolds for bone tissue regeneration. *J. Biomater. Sci. Polym. Ed.* **2013**, *24*, 1988−2005.
(61) Sharif, F.; Porta, F.; Meijer, A. H.; Kros, A.; Richardson, M. K. Mesoporous silica nanoparticles as a compound delivery system in zebrafish embryos. *Int. J. Nanomed.* **2012**, *7*, 1875−1890.
(62) Zhao, Y.; Shen, Y.; Bai, L. Effect of chemical modification on carbon dioxide adsorption property of mesoporous silica. *J. Colloid Interface Sci.* **2012**, *379*, 94−100.
(63) Chrissafis, K.; Antoniadis, G.; Paraskevopoulos, K. M.; Vassiliou, A.; Bikiaris, D. N. Comparative study of the effect of different nanoparticles on the mechanical properties and thermal degradation mechanism of in situ prepared poly(ε-caprolactone) nanocomposites. *Compos. Sci. Technol.* **2007**, *67*, 2165−2174.
(64) Solomon, O. F.; Ciută, I. Z. Détermination de la viscosité intrinsèque de solutions de polymères par une simple détermination de la viscosité. *J. Appl. Polym. Sci.* **1962**, *6*, 683−686.
(65) Kirsh, Y. E.; Yanul, N. A.; Kalninsh, K. K. Structural transformations and water associate interactions in poly-N-vinylcaprolactam−water system. *Eur. Polym. J.* **1999**, *35*, 305−316.
(66) Meeussen, F.; Nies, E.; Berghmans, H.; Verbrugghe, S.; Goethals, E.; Du Prez, F. Phase behaviour of poly(*N*-vinyl caprolactam) in water. *Polymer* **2000**, *41*, 8597−8602.
(67) Pace, C. N. Conformational stability of globular proteins. *Trends Biochem. Sci.* **1990**, *15*, 14−17.
(68) Alf, M. E.; Hatton, T. A.; Gleason, K. K. Insights into Thin, Thermally Responsive Polymer Layers Through Quartz Crystal Microbalance with Dissipation. *Langmuir* **2011**, *27*, 10691−10698.
(69) Tiktopulo, E. I.; Bychkova, V. E.; Ricka, J.; Ptitsyn, O. B. Cooperativity of the Coil-Globule Transition in a Homopolymer: Microcalorimetric Study of Poly(N-isopropylacrylamide). *Macromolecules* **1994**, *27*, 2879−2882.
(70) Fuciños, C.; Fuciños, P.; Míguez, M.; Katime, I.; Pastrana, L. M.; Rúa, M. L. Temperature- and pH-Sensitive Nanohydrogels of Poly(*N*-Isopropylacrylamide) for Food Packaging Applications: Modelling the Swelling-Collapse Behaviour. *PLoS One* **2014**, *9*, No. e87190.
(71) Patenaude, M.; Hoare, T. Injectable, Degradable Thermoresponsive Poly(*N*-isopropylacrylamide) Hydrogels. *ACS Macro Lett.* **2012**, *1*, 409−413.
(72) Charlet, G.; Ducasse, R.; Delmas, G. Thermodynamic properties of polyolefin solutions at high temperature: 2. Lower critical solubility temperatures for polybutene-1, polypentene-1 and poly(4-methylpentene-1) in hydrocarbon solvents and determination of the polymer-solvent interaction parameter for PB1 and one ethylene-propylene copolymer. *Polymer* **1981**, *22*, 1190−1198.
(73) Sala, R. L.; Arantes, T. M.; Longo, E.; Leite, E. R.; Paranhos, C. M.; Camargo, E. R. Evaluation of modified silica nanoparticles in carboxylated nitrile rubber nanocomposites. *Colloids Surf., A* **2014**, *462*, 45−51.
(74) Park, S. J.; Cho, M. S.; Lim, S. T.; Choi, H. J.; Jhon, M. S. Synthesis and Dispersion Characteristics of Multi-Walled Carbon Nanotube Composites with Poly(methyl methacrylate) Prepared by In-Situ Bulk Polymerization. *Macromol. Rapid Commun.* **2003**, *24*, 1070−1073.
(75) Heatley, F. Nuclear magnetic relaxation of synthetic polymers in dilute solution. *Prog. Nucl. Magn. Reson. Spectrosc.* **1979**, *13*, 47−85.
(76) Lússe, S.; Arnold, K. The Interaction of Poly(ethylene glycol) with Water Studied by ^{1}H and ^{2}H NMR Relaxation Time Measurements. *Macromolecules* **1996**, *29*, 4251−4257.
(77) Bloembergen, N.; Purcell, E. M.; Pound, R. V. Relaxation Effects in Nuclear Magnetic Resonance Absorption. *Phys. Rev.* **1948**, *73*, 679−712.
(78) Munie, G. C.; Jonas, J.; Rowland, T. J. NMR relaxation study of crosslinked *cis*-1,4-polybutadiene. *J. Polym. Sci., Part A: Polym. Chem.* **1980**, *18*, 1061−1070.

https://dx.doi.org/10.1021/acs.langmuir.0c03079
Langmuir 2021, 37, 1531−1541